



UNIVERSITY OF LEEDS

This is a repository copy of *Enabling internal electronic circuitry within additively manufactured metal structures - The effect and importance of inter-laminar topography*.

White Rose Research Online URL for this paper:
<http://eprints.whiterose.ac.uk/114243/>

Version: Accepted Version

Article:

Li, J, Monaghan, T, Kay, R et al. (2 more authors) (2018) Enabling internal electronic circuitry within additively manufactured metal structures - The effect and importance of inter-laminar topography. *Rapid Prototyping Journal*, 24 (1). pp. 204-213. ISSN 1355-2546

<https://doi.org/10.1108/RPJ-08-2016-0135>

© Emerald Publishing Limited 2018. This is an author produced version of a paper published in *Rapid Prototyping Journal*. Uploaded in accordance with the publisher's self-archiving policy.

Reuse

Items deposited in White Rose Research Online are protected by copyright, with all rights reserved unless indicated otherwise. They may be downloaded and/or printed for private study, or other acts as permitted by national copyright laws. The publisher or other rights holders may allow further reproduction and re-use of the full text version. This is indicated by the licence information on the White Rose Research Online record for the item.

Takedown

If you consider content in White Rose Research Online to be in breach of UK law, please notify us by emailing eprints@whiterose.ac.uk including the URL of the record and the reason for the withdrawal request.



eprints@whiterose.ac.uk
<https://eprints.whiterose.ac.uk/>

Optimising the interlaminar geometry of ultrasonically additive manufactured metal structures to enable direct embedding of electronic circuitries

J. Li*, T. Monaghan, R.W. Kay, R.J. Friel, R.A. Harris

Email: J.li5@Lboro.ac.uk Tel: +44(0)1509227567

Wolfson School of Mechanical and Manufacturing Engineering, Loughborough University, Loughborough, Leicestershire, LE11 3TU, UK

Abstract

Purpose - This research aims to exploit the potential of Ultrasonic Additive Manufacturing (UAM) in the embedding of printed electrical materials directly into the interlaminar region of parts during manufacture in order to realise novel multifunctional Metal Matrix Composite's (MMC's).

Design/methodology/approach - To ensure the proper electrical insulation between the printed conductor and metal matrices, an insulation layer with sufficient thickness is required to adapt the rough interlaminar surface geometry caused by the transfer of the sonotrode topography during the UAM process. This in turn increases the total thickness of printed circuitries and thereby adversely affects the integrity of the UAM part. This work proposes a unique solution to overcome this rough interlaminar surface through deformation of the UAM substrates via sonotrode rolling or UAM processing.

Findings - The surface roughness (S_a) of UAM substrates could be reduced from 4.5 μm to 4.1 μm by sonotrode rolling and from 4.5 μm to 0.8 μm by ultrasonic deformation. Peel testing demonstrated that sonotrode rolled substrates could maintain their mechanical strength, whilst the performance of substrates deformed with UAM degraded under same welding conditions (~12% reduction compared with undeformed substrates). This observation was attributed to the work hardening effect of deformation process which was identified via DualBeam FIB-SEM investigation.

Originality/value - The rolling deformation process (without ultrasonic assistance) was adopted in the further fabrication of multifunctional MMC's. This method enabled a decrease in the thickness of printed electrical circuitries by ca. 25%.

Keywords: Ultrasonic Additive Manufacturing (UAM); 3D Printing; Topography; Grain refinement; Metal Matrix Composite (MMC); Mechanical strength

* Corresponding author.

1. Introduction

Ultrasonic Additive Manufacturing (UAM) is a solid-state additive manufacturing technology which applies Ultrasonic Metal Welding (UMW) to join metal foils to one another in a layer by layer manufacturing process. Periodic Computer Numerical Control (CNC) machining is then implemented (either post-process or during manufacture) to create complex 3D metal structures (White, 2003) (Fig. 1). A rotating sonotrode is used to transfer ultrasonic oscillations generated from an ultrasonic transducer and apply a normal pressure to maintain intimate foil-foil/substrate-foil contact. The induced friction at the welding interface in combination with plastic deformation of the adjacent metal beneath the points of intimate contact act to disperse the surface oxide layer and create more metal-to-metal connections. The result of the applied pressure and ultrasonic oscillation is the formation of a metallurgical bond along the welding interface (Kong et al., 2005). Three control parameters: normal force (N), ultrasonic oscillation amplitude (μm), and welding speed (mm/s), are used to regulate the applied UAM welding energy.

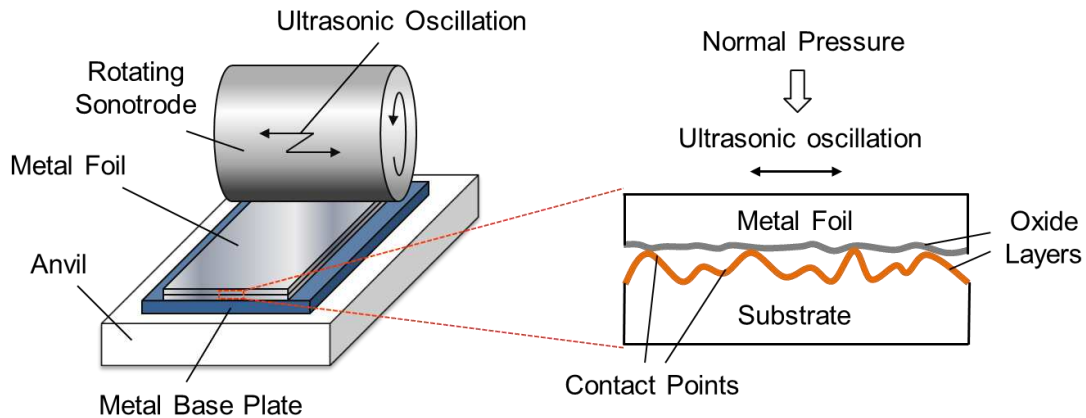


Fig. 1. Schematic drawing of Ultrasonic Additive Manufacturing (UAM).

In the UAM process, the bulk temperature increase is much lower than the melting point of the metals to be consolidated. Furthermore, significant plastic flow of the metal matrix also occurs at the welding interface. Both these key features have demonstrated their ability to enable the embedding of thermally sensitive electrical components via UAM (Kong and Soar, 2005; Mou et al., 2009; Robinson et al., 2006; Siggard et al., 2006). In the authors previous work, the feasibility of direct embedding of printed electrical materials within UAM metal structures was investigated with promising results (Li et al., 2015). However, a challenge relating to the UAM interlaminar surface geometry hindered the embedding of optimal functional electrical circuitries. The impingement of the sonotrode during UAM processing produces a significantly rougher texture on the top surface of the welded foil (as compared to the pre-processed foil surface). This rougher surface is not an ideal substrate for the subsequent printing of electrical pathways and production of MMC components. To ensure functionality of the printed conductors, relatively thick (ca. 30 μm) shrouding polymer insulation material must be deposited onto the UAM sample surface to adapt

the inter-UAM foil surface geometry and avoid electrical shortages between the UAM metal matrices and the printed conductors. This necessity increases the total thickness of the electrical components embedded in the UAM samples which reduces the overall mechanical integrity of the final structure (Li et al., 2014, 2015).

This research presents an innovative surface deformation process via sonotrode rolling or ultrasonic processing to overcome the negative effects of the interlaminar UAM surface geometry when creating MMC components with integrated circuitry. The effects of the deformation process on UAM structure are also systematically investigated in this paper.

2. Experimental procedure

2.1. Surface deformation process

The method of surface deformation is demonstrated in Fig. 2. Firstly, two aluminium (Al) 3003 H18 foils at $\sim 100 \mu\text{m}$ thick and $\sim 24 \text{ mm}$ wide were sequentially UAM welded onto an Al 1050 H14 base plate with a thickness of $\sim 1.2 \text{ mm}$ and width $\sim 30 \text{ mm}$, at room temperature (Fig. 2 (a)). The UAM apparatus used in this study was the Alpha 2 UAM machine supplied by Solidica INC. (USA) which is capable of providing an output power of 2 kW and a frequency of $\sim 20 \text{ kHz}$. The UAM parameters used were 1400 N weld pressure, $20 \mu\text{m}$ sonotrode amplitude, and 40 mm/s welding speed, respectively. These parameters were chosen as a result of prior systematic tests and work focusing on the UAM processing of 3003 H18 aluminium (Janaki Ram et al., 2006; Kong et al., 2004; Kulakov and Rack, 2009)..

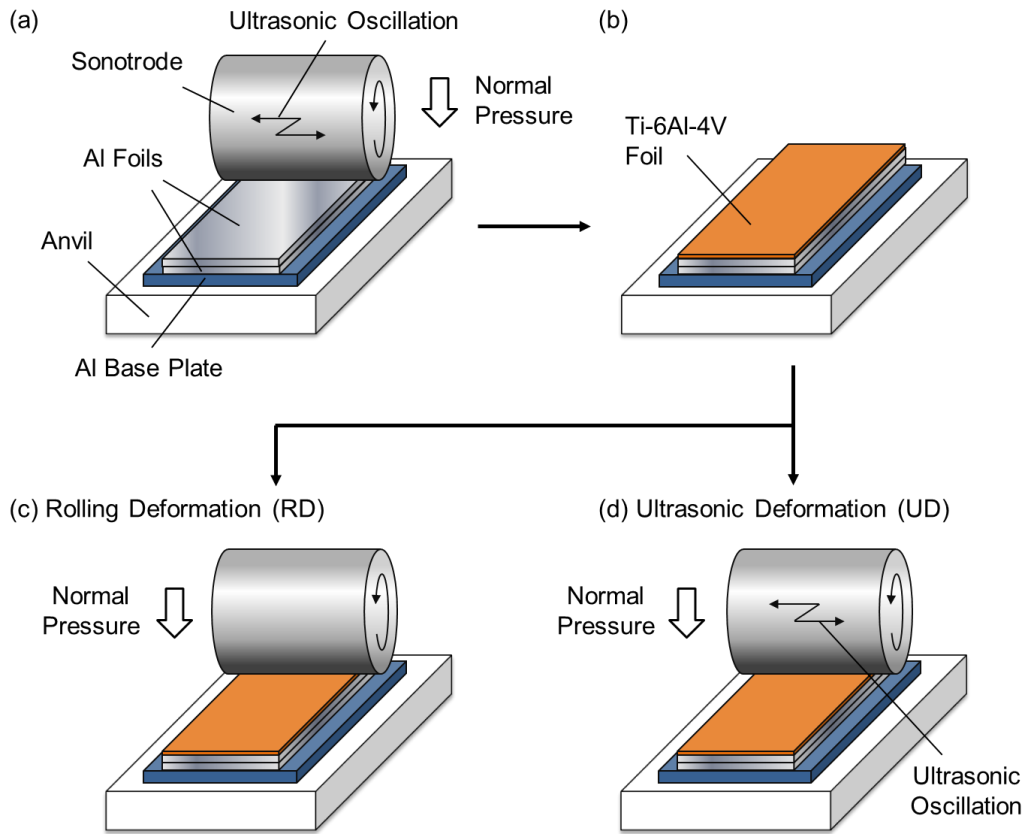


Fig. 2. Process chain of surface deformation process.

Following this, a 50 μm thick and 24 mm wide Ti-6Al-4V foil was placed on the top surface of UAM fabricated substrate (Fig. 2 (b)). After that, two types of deformation process were investigated using the described UAM apparatus. The first one was termed Rolling Deformation (RD) was employed in which only normal pressure was applied to the Ti-6Al-4V foil via the rotating sonotrode (Fig. 2 (c)). Secondly Ultrasonic Deformation (UD) whereby both ultrasonic oscillation and normal pressure were exerted on the titanium foil via the rotating sonotrode in a method similar to normal UAM welding procedures (Fig. 2 (d)). Due to the contribution of ultrasonic energy, it was hypothesised that the UD process could more effectively deform the surface geometry of UAM processed substrate to create a much smoother surface texture. For each type, two combinations of control parameters were used as stated in Table 1.

Table 1. The combinations of control parameters used to modify UAM substrate surface texture.

	Serial Number	Weld force (N)	Welding speed (mm/s)	Sonotrode amplitude (μm)
Ultrasonic deformation (UD)	UD1	800	20	12
	UD2	1400	40	20

Rolling deformation (RD)	RD1	800	20	—
	RD2	1400	40	—

2.2. Modifications of deformation process on UAM interlaminar surface

It was hypothesised that the aforementioned deformation processes could cause surface topography modification and grain refinement on the UAM fabricated substrate. These modifications may therefore act to alter the bonding strength of UAM metal matrices. Therefore, these two potential issues were investigated via non-contact focus variation microscopy (Infinite Focus, Alicona Imaging GmbH, Grambach, Austria) and Dual Beam Focused Ion Beam - Scanning Electron Microscope (Nova 600 Nanolab, FEI, Oregon, USA).

2.2.1 Surface topography

To explore the change of surface topography, the UAM substrate surfaces (undeformed and deformed) were investigated using an Alicona InfiniteFocus® G4f, an optical 3D Infinite Focus Microscope (IFM). The object lens used for measuring was a $\times 20$ lens. It provided a field view of $715 \mu\text{m}$ in the horizontal (X axis) by $544 \mu\text{m}$ in the vertical (Y axis). For each parameter set of each deformation process, three samples were measured and a total of five scanning areas taken along the central line of each sample (Fig. 3). The dimensions of each area are 1.97 mm in length and 1.90 mm in width. Three undeformed samples were also measured using the same methodology in order to act as a comparative reference.

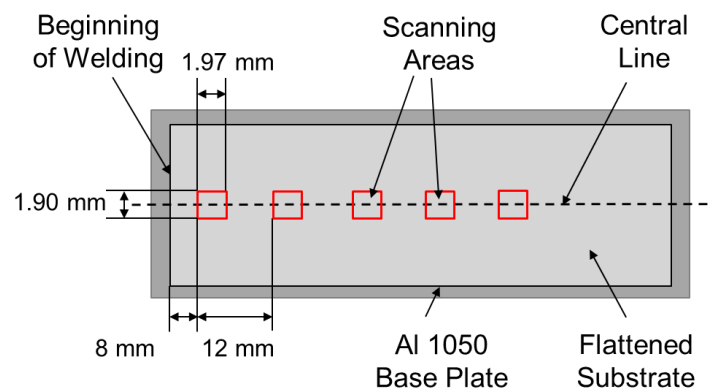


Fig. 3. Schematic demonstrating the various regions sampled for topography analysis via the Alicona InfiniteFocus® G4f focus variation microscopy setup.

The selected scanning areas were chosen based on two principles: firstly, the Alpha 2 UAM machine shows a delay small time period to achieve the pre-set working conditions after the machine is initiated. As a result, the first several millimetres bonding were considered to be non-representative of the true welding surface at these

parameter combinations. Thus the first area was taken at the position 8 mm from the beginning of the bonding. Secondly, experience gained in previous peel testing displayed that foil fractures typically occurred in a range of 20 to 40 mm from the point of initial consolidation (Monaghan et al., 2015). In light of this, a series of surface scanning areas were selected to cover this range and thus reveal any correlation between mechanical strength of the UAM metal matrices and the topography of the substrate.

2.2.2 Surface grain refinement

It was theorised that the mechanical and thermal stresses induced during the surface deformation process may act to increase the micro-hardness (work hardening) of the UAM interlaminar surface via grain-boundary strengthening (or Hall–Petch strengthening) and as a result, may affect the ability to weld successive foil layer. Grain-boundary strengthening is a phenomenon that results in increases in strength of a material by reducing their average crystallite grain size. Theoretically, decreasing the grain size creates more grain boundaries that impede dislocation movement, and reduces dislocation pile up within a grain, leading to a lower driving force for dislocations to move from one grain to another. This in turn leads to a strengthening of the material. The relation between work hardening and grain size is described by the Hall–Petch equation (Smith and Hashemi, 2006):

$$\sigma_y = \sigma_0 + \frac{k_y}{\sqrt{d}} \quad (1)$$

where σ_y is the yield stress, σ_0 is a materials constant for the resistance of the lattice to dislocation motion, k_y is the strengthening coefficient that is a constant specific to each material, and d is the average grain diameter.

Therefore, any possible surface work hardening due to deformation process could be identified via investigating the grain size in the area beneath the deformed surface. The most applicable method based on prior literature is Focussed Ion Beam (FIB) milling in combination with Dual SEM imaging in order to analyse and assess the grain structure of the processed materials (Friel and Harris, 2010). This was performed through the use of a Nova 600 Nanolab Dual Beam Focused Ion Beam - Scanning Electron Microscope (FEI, Oregon, USA). This instrument consists of a high resolution field emission electron column and gallium source ion column combined within the same instrument. This allows for the milling of cross sections through samples, and the subsequent imaging of these trenches using either electrons or ions. Ion beam milling was used to produce a 10 μm wide, 20 μm long and 10 μm deep trench parallel to the flattened surface of the processed foil. This was performed for both RD and UD samples along with a reference non-flattened sample. Once milled, the interface was then imaged at high resolution via the use of the inbuilt dual ion beam imaging and SEM functions.

2.3. Effects of deformation process on the mechanical strength of UAM metal matrices

An Al 3003 H18 cover foil was welded directly onto the flattened UAM substrates (processed with the different parameter sets) and the aspects of mechanical strength systematically investigated via peel testing and optical microscopy. This allowed quantification of any influence of the deformation process, in combination with UAM welding parameters on the strength of the UAM fabricated structures. Two sets of welding parameters were used to weld this final layer: a High Energy set (HE) (1400 N normal force, 20 μm sonotrode amplitude, and 40 mm/s welding speed) which is identical to that used for substrate fabrication (section 2.1), and a Low Energy set (LE) (800 N normal force, 12 μm sonotrode amplitude, and 20 mm/s welding speed). According to the analytical energy model built by Yang et al. (Yang et al., 2010), the energy density of the HE and LE UAM parameter combinations is 0.7 J/mm² and 0.48 J/mm², respectively. Therefore a significant energy difference exists between the two parameter sets to highlight any differences which arise as a result of the processing energy on the mechanical strength of the final UAM structure.

2.3.1 Optical microscopy

Optical microscopy was used to investigate the mechanical strength through quantification of the interlaminar bond density. The term Linear Weld Density (LWD) describes the percentage of bonded area along the weld interface and can be obtained from optical microscopy images of UAM welded cross-sections. LWD can be expressed as:

$$LWD(\%) = \frac{L_b}{L_i} \times 100 \quad (2)$$

where L_b and L_i are the length of the bonded area and the length of total bond interface, respectively.

For each type of flattened substrate and each UAM welding parameter combination, two samples were cross-sectioned and measured using a Nikon Eclipse MA200 optical microscope with a $\times 10$ object lens. Four non-flattened samples were also prepared and cross-sectioned for comparative reference. Each sample was cut into three sections (front, middle, and rear) which were cold mounted in epoxy resin and then gradually ground and polished to 0.05 μm finish (Fig. 4). For each mounted section, eight images were taken from the weld interface between cover foil and UAM substrate. In total, 240 images were measured in this test.

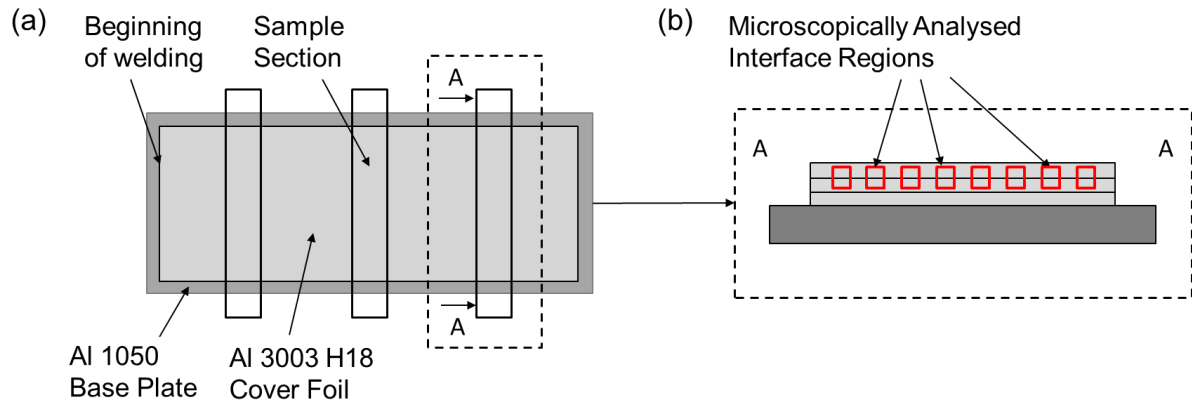


Fig. 4. (a) Typical regions cross sectioned and taken forward to mounting/polishing; (b) regions analysed for assessment of samples LWD.

2.3.2 Mechanical peel testing

Peel testing was performed in accordance with the requirements of BS EN 2243-2 2005, as demonstrated in Fig. 5. All samples were mounted into a peeling jig attached to an Instron 5500R tensile test machine. The free end of the cover foil was clamped by a chuck whilst the substrate was held stationary by the peeling jig. In the act of peeling, the chuck moved downwards at a constant velocity of 50 mm/min in order to apply a tensile load to the cover foil and peel it from the underlying substrate. Peeling was set to stop when the peeling load dropped to 10% of the maximum value attained for the sample.

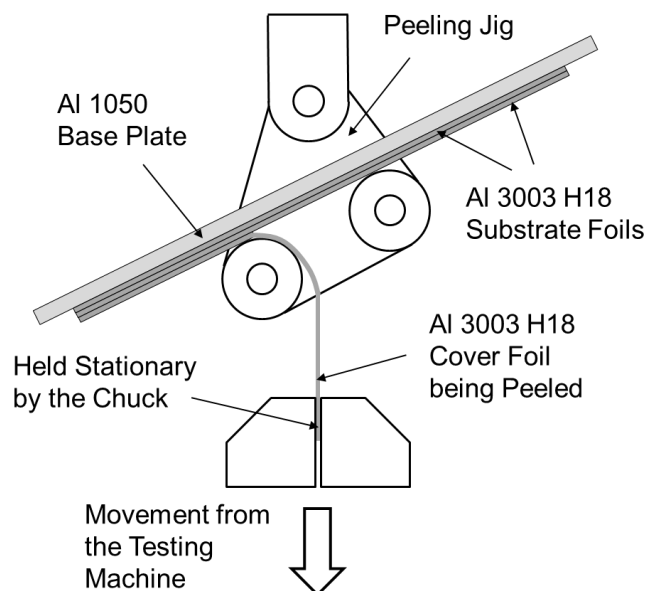


Fig. 5. Schematic drawing of peel testing apparatus and setup.

For each parameter combination of the deformation process and UAM welding parameter set, six samples were peeled to obtain an average value of the maximum peel load. Twelve unmodified UAM substrates were also capped with both UAM energy sets and then tested in the same way for comparative reference.

3. Results and Discussion

3.1. Modifications of deformation process on UAM interlaminar surface

3.1.1 Surface topography of UAM interlaminar surface

Surface flattening was performed in accordance with Section 2.1. No Al to Ti foil bonding was noted during the experiments although Obielodan et al. have previously reported that softer pure titanium foils can be ultrasonically welded onto various aluminium alloys (Al 3003-H18 and Al 6061-0) (Obielodan et al., 2010). This is attributed to the lower output power of the UAM equipment used in this work in combination with the higher material hardness of Ti-6Al-4V. The Ti foil was thus regarded as a flattening tool in this process as opposed to a potential bonding layer. The topography of UAM substrates were scanned using an Alicona InfiniteFocus® G4f as detailed in Section 2.3, and the obtained files were studied with TalyMap Platinum 5.0 software. Representative surface topographies of undeformed and rolling deformed substrates are demonstrated in Fig. 6.

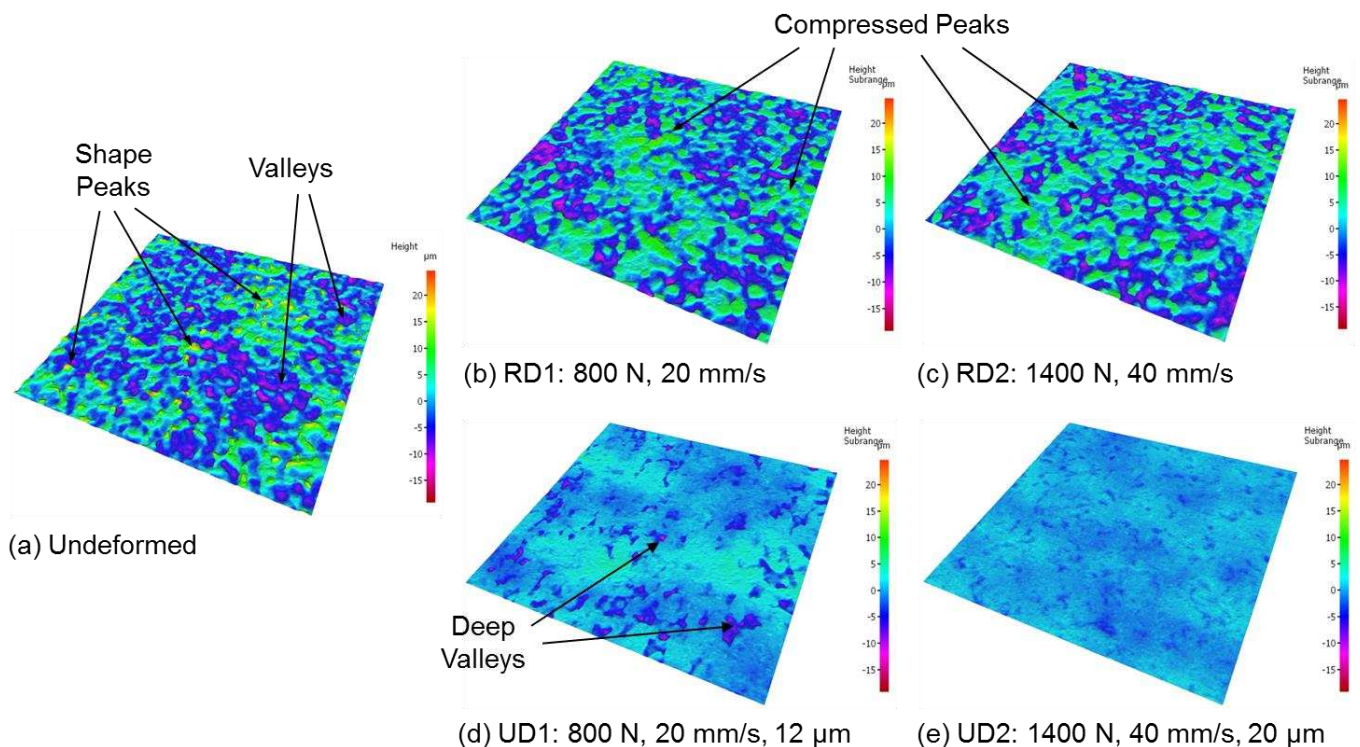


Fig. 6. Surface topographies of UAM substrate from Alicona InfiniteFocus® G4f investigation: (a) undeformed; (b) rolling deformed with RD1; (c) rolling deformed with RD2; (d) ultrasonically deformed with UD1; and (e) ultrasonically deformed with UD2.

As Fig. 6 (a) demonstrates, undeformed substrates exhibited distinctly rougher surfaces with numerous peaks and valleys. With the RD process, the larger of these peaks appear to have been compressed by the normal force of the sonotrode, leaving behind a surface which still exhibits a distinct roughness, but with fewer extremes in the form of these large surface peaks.

In contrast, substrates processed with the various UD parameter combinations possessed significantly deformed surfaces to yield a significantly flatter profile. In the lower energy combinations (UD1) some deep valleys were still noted on the surface (Fig. 6 (d).) Higher UAM flattening energy (UD2) acted to significantly increase this deformation effect and further reduce the observed surface roughness (Fig. 6 (e)). This effect was attributed to increase plastic flow being induced into the matrix material which when combined with the sonotrodes normal force, softened and displaced material from the rough surface peaks into the surrounding valleys. Thus, with the assistance of ultrasonic oscillation, the deformation process was more effective in reducing the surface roughness.

The average surface roughness (S_a) change with regards to the distance from the welding start point is plotted in Fig. 7. For the undeformed surfaces, S_a increased rapidly in the starting area of the welding, and then gradually reached a value of ca. $4.5 \mu\text{m}$. Thus the trend of the S_a indicated that UAM apparatus required a certain time to achieve a stable pre-set working condition and create a uniformly rough surface. The roughness of the rolling deformed surface displayed a similar tendency to that of an undeformed surface, but the final value was shown to gradually decrease to ca. $4.1 \mu\text{m}$ following the application of increasing rolling stress.

For the samples deformed with UD1, the S_a was shown to increase with a corresponding increase of welding distance. However, the change of final surface roughness was significantly reduced to $2.2 \mu\text{m}$ when compared to the original value of the unprocessed foil. Unlike UD1, S_a of UD2 grew slightly and then demonstrated a notable decrease in S_a to ca. $0.8 \mu\text{m}$, less than 1/5th of the original value or the unprocessed foil. This was attributed to the larger UAM processing energy of UD 2 being sufficient enough to compress and deform the roughness of the substrate even in the beginning of the UAM flattening process.

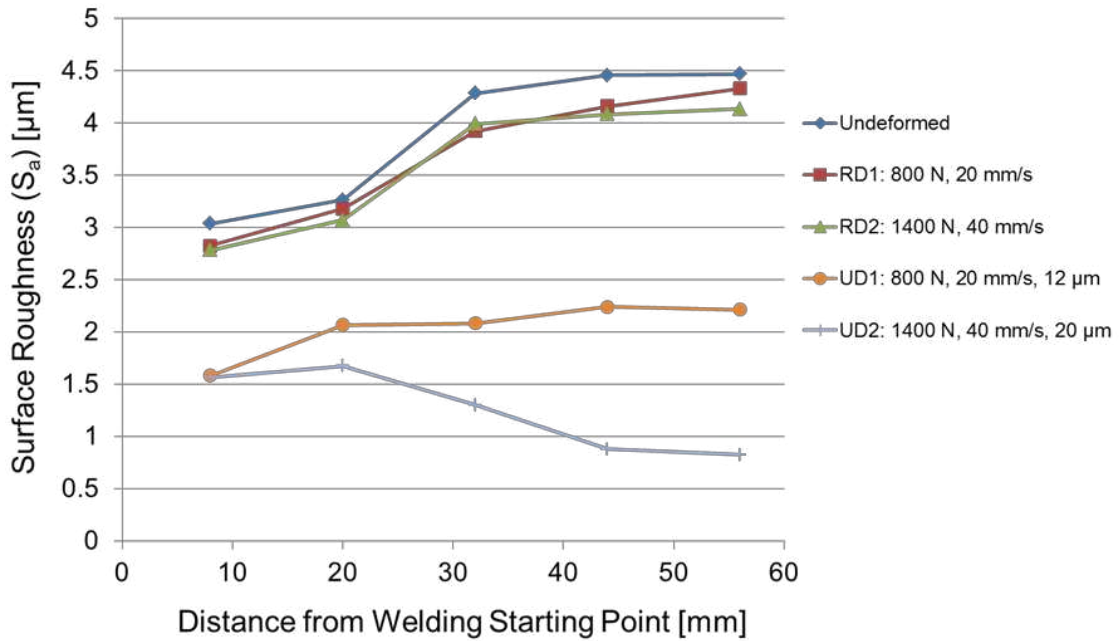


Fig. 7. The average surface roughness S_a changing with respect to the welding start position.

Despite a small change in S_a when comparing the undeformed and RD samples, analysis of the mean surface maximum peak height (R_p) shows a significant decrease after processing (Fig. 8). This trend supports the observations based upon the topographical images displayed in Fig. 6(b) and (c) that surface peaks were significantly affected during the RD process. Therefore RD samples are able to maintain a significantly rough surface whilst eliminating the most significantly obtrusive peaks. The RD samples were therefore able to produce an R_p value of around $8 \mu\text{m}$, with slight reductions coming by way of increased normal force. In comparison, samples prepared using UD again exhibited amplified results. Here almost all of the peaks present on the surface were reduced to leave an R_p value less than $4 \mu\text{m}$, with decreases in peak height coming by way of increased ultrasonic energy.

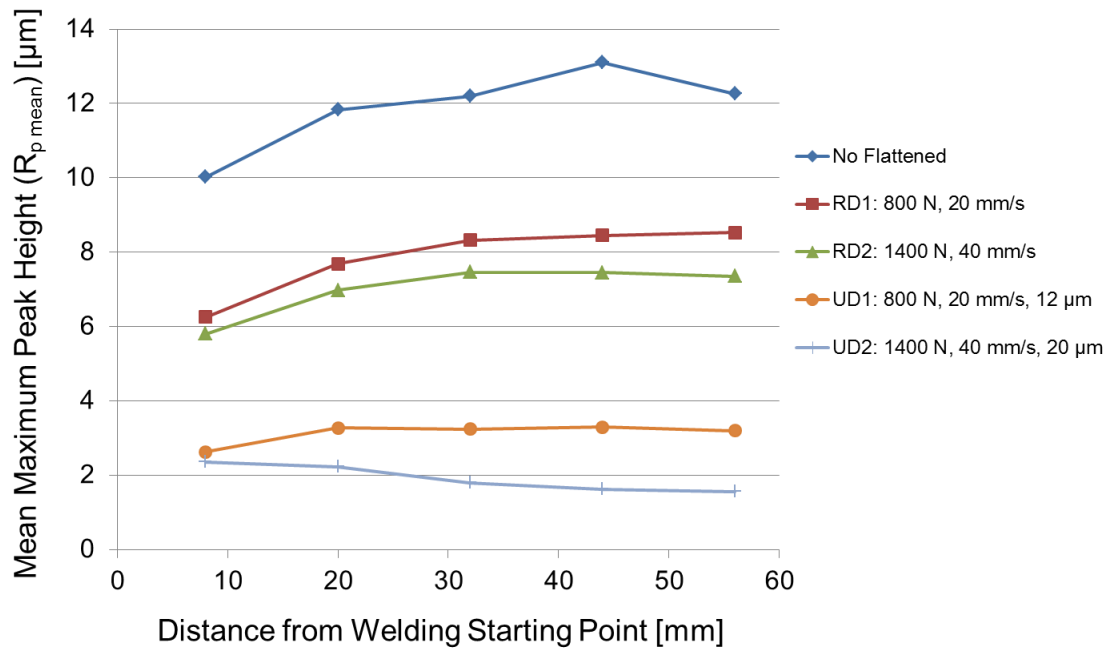


Fig. 8. Mean maximum peak height (R_p) changing with respect to the welding start position

Analysis of the substrates R_v values, which analyses the mean maximum mean valley depth support these findings. The R_v value of RD samples were seen to only change a small amount when compared to the undeformed sample. This is because the compressive force of the sonotrode was not great enough to fully displace the compressed peaks into the surrounding valleys. However samples processed using the UD combinations resulted in more dramatic reductions in R_v . Samples prepared using the UD2 combinations were able to achieve R_v values of ca. 2.2 μm .

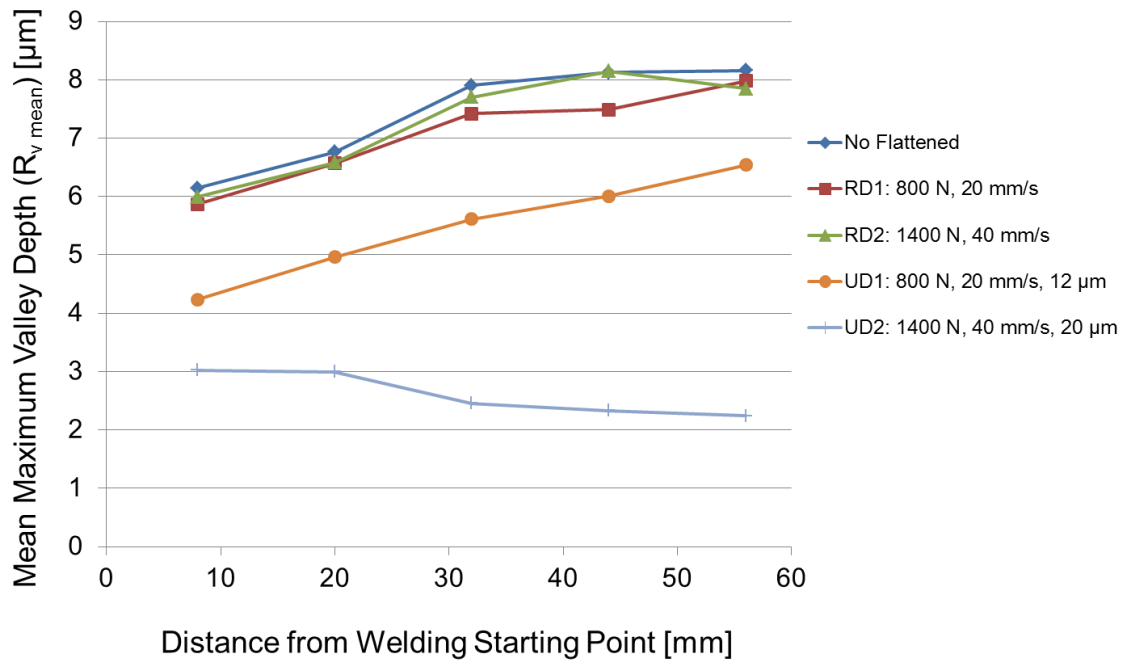


Fig. 9. Mean maximum valley depth (R_v) changing with respect to the welding start position.

Analysis of the substrates R_z values, which analyses the mean maximum peak-to-height distance, indicated that all of these surface deformation procedures would be suitable for future works in the embedding of electrical circuitries (Fig. 10). In these instances, it is desirable to use as few layers of insulating dielectric material as possible. Providing the thickness of this dielectric layer is greater than the R_z value, it should therefore be capable of adapting to the modified UAM substrates surface to provide electrical insulation and prevent the occurrence shortages. This is also able to occur whilst simultaneously reduction the height of the embedded structure. This application is discussed in more detail in Section 3.3.

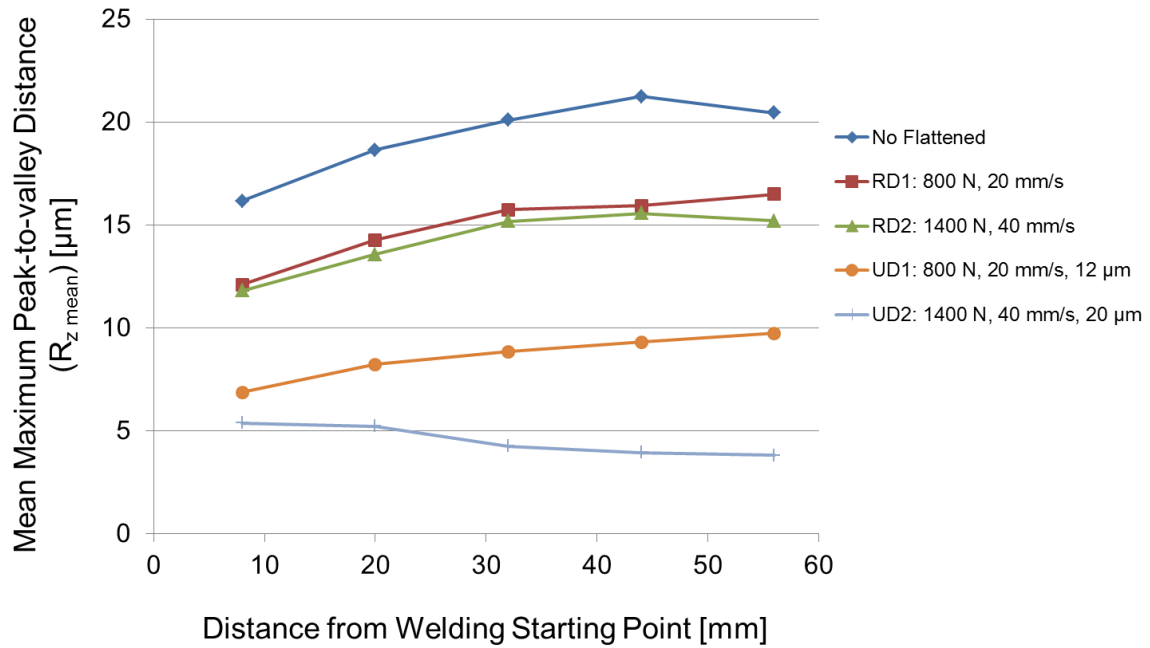


Fig. 10. Mean maximum peak-to-valley distance (R_z) changing with respect to the welding start position.

3.1.2 Surface work hardening due to the deformation process

Several researchers have noted work hardening of Aluminium matrices as a result of UAM (Li and Soar, 2008). Through the action of plastic flow observed in UAM, dislocations display higher density with an accompanying reduction in mobility. As a result, increases in material strength and hardness are often observed. At higher contact pressures and oscillation amplitudes, this effect is amplified due to increasing degrees of plastic flow observed in the matrix material resulting in a harder, stronger material post-processing. As a result, these materials are often less susceptible to bond formation via UAM due to reduced plastic flow and a more stubborn oxide layer (Jenney and O'Brien, 1991).

Through the use of dual FIB-SEM, highly magnified ion beam images at the surface of the undeformed and RD foils are shown in Fig. 11. Fig. 11 (a) shows a thin refined grain layer (less than 0.5 μm) on the surface of undeformed which is typical of UAM processed foils. Due to the 'rounding off', but not complete deformation of sharp 'peaks' on the surface of the RD processed substrate (shown in Fig. 11 (b)), the Ti foil (pressed by sonotrode) is prone to contact the upper most point of the surface more so than the 'valleys'. Fig. 11(b) demonstrates that the tips of these surface peaks display a higher

degree of grain refinement than the bulk matrix and the valley area, which appear to retain their larger grain size.

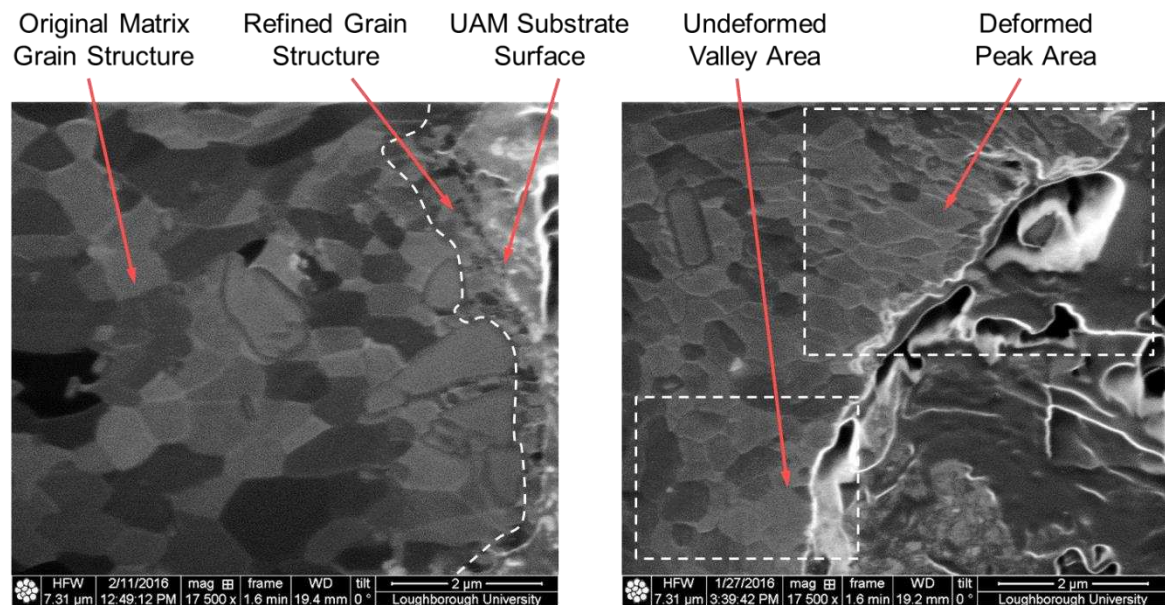


Fig. 11. (a) Grain structure of undeformed Al 3003 H18 substrate; (b) Effect of RD2 deformation condition on the grain structure of Al 3003 H18.

In contrast to this partial refinement, the ultrasonically deformed samples, which possess a much smoother surface, demonstrated a different tendency. Ion beam imaging revealed that the application of ultrasonic energy during the deformation process lead to a significantly larger degree of grain refinement in the uppermost regions of the foil – Fig. 12(a). Compared with undeformed samples, this refined region was exhibited in a much thicker distinct band stretching the length of the surface, with an approximate depth of 2-3 μm . As this surface is almost completely flat, it was assumed that all points of the surface contacted the Ti foil in much the same way, and were therefore subject to the same grain refinement. In the substrates deformed using the UD2 parameters, SEM micrographs highlighted the formation of several cracks on the surface of the substrates. The emergence of these cracks was attributed to the apparent increase in material hardness in the upper foil region – Fig. 12(b). This increase will lead to residual stresses in the foil as a result of the boundary between the refined and unrefined region, leading to eventual cracking along this boundary during the rolling and oscillation of the sonotrode.

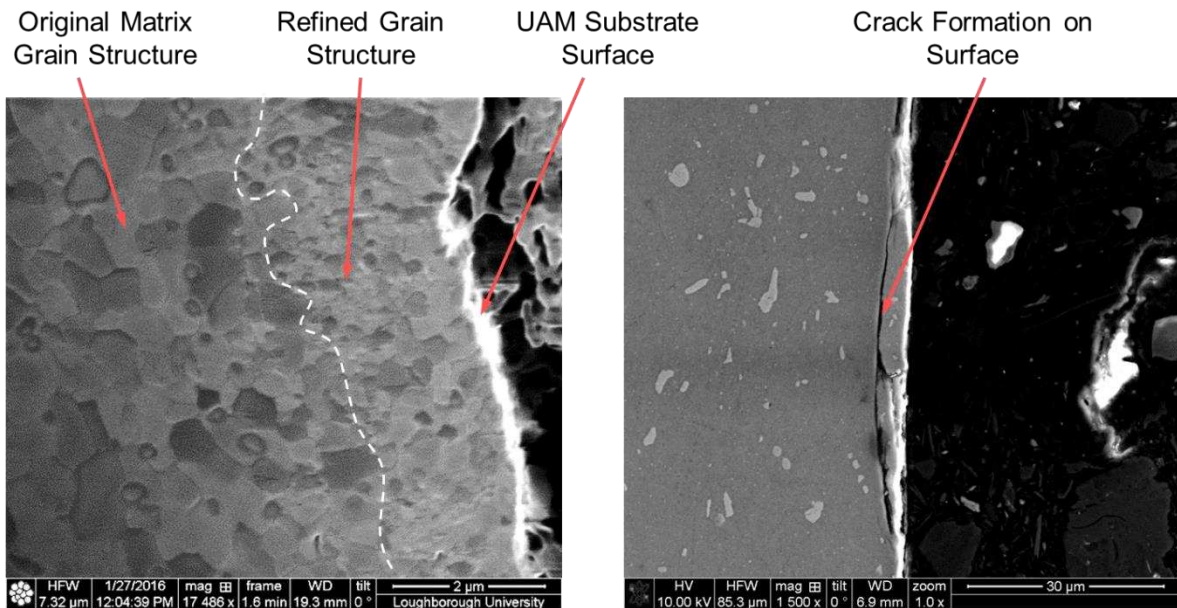


Fig. 12. (a) Effect of UD2 deformation conditions on the grain structure of Al 3003 H18; (b) crack formation in samples flattened using UD2 parameters.

Therefore, with rolling deformation process the upper most foil is predominately comprised of unrefined grain regions and is therefore softer and more susceptible to bonding during UAM. The ultrasonic deformation process led to a distinct work-hardened band extending the length of the surface, resulting in the matrix being less susceptible to the ultrasonic consolidation of subsequent foil layers. It was important to confirm the effect of this grain refinement on the mechanical properties of the resulting UAM parts when these successive foils were welded on the different surfaces. In light of this, a combination of optical microscopy and mechanical peel testing were implemented to establish if there was any variation in mechanical properties as a result of these various surface flattening methods.

3.2. Quantifying the effect of the deformation process on the mechanical strength of UAM metal matrices

3.2.1 Optical microscopy

Linear Weld Density (LWD) measurements of both the undeformed and deformed samples welded using both UAM energy sets are shown in Fig. 13. Generally, higher UAM energies resulted in higher LWD values ($\geq 95\%$) and much smaller standard error for each sample categories when compared to their lower UAM energy counterparts. The LWD of the samples welded through the use of high UAM energy rose slightly with the decrease of surface roughness S_a caused by the deformation process. For the low UAM energy sets, the tendency of LWD was not so clear. However, it was still found that most deformed samples exhibited larger LWD than the original samples. When UAM flattening was applied, the LWD increased from 84% for undeformed samples up to ca. 90%.

These results demonstrated that the surface deformation process was able to improve the LWD of the UAM structures. This was attributed to the surface deformation of the substrate surface which arises due to the use of an intermediary titanium alloy layer. Due to this deformation, the peaks on the substrate were compressed, making the valleys shallower. Therefore, minor plastic flow driven by UAM welding was adequate enough to fill the valleys/voids. This enhanced LWD and avoided the stress intensity on the edges of the voids in the welding interface, which could lead to potential improvements in the structural integrity and mechanical strength of UAM metal components.

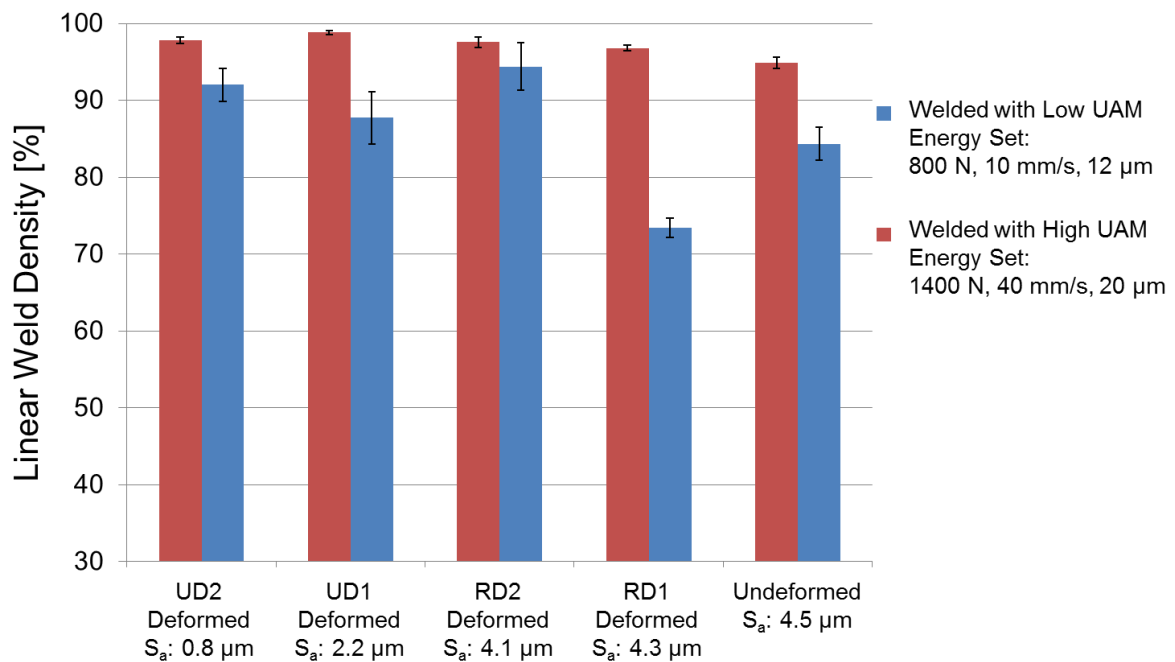


Fig. 13. Linear weld density for undeformed and deformed samples.

3.2.2 Mechanical peel performance

Al 3003 H18 cover foils were welded using high and low UAM energy parameter combinations on to the surface of the substrates which were both undeformed and deformed using UD1, UD2, RD1, and RD2 parameter sets. All of these samples were peel tested in accordance with BS EN 2243-2 2005. The average maximum peeling loads with their respective standard errors are shown in Fig. 14.

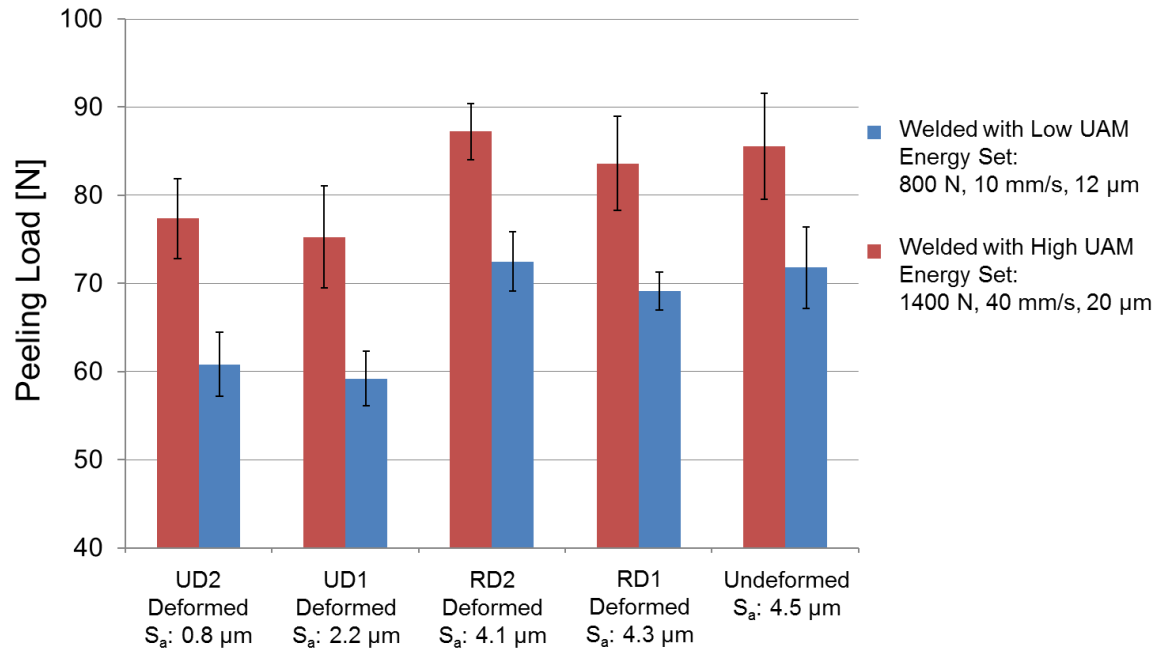


Fig. 14. The average maximum peeling loads for undeformed and deformed samples.

For all types of UAM substrates, the peeling loads for higher UAM energy were ca. 15 N larger than those capped by lower UAM energy. The samples deformed using both RD1 and RD2 parameters display almost identical peeling load as the unflattened samples, ca. 70 N for low UAM energy welding set and 85 N for high energy. However, compared with undeformed samples, there was a remarkable reduction of peeling load of both UAM flattened categories by ca. 14% and 12% for low and high UAM energy sets respectively. Hence, it can be deduced that rolling deformation is capable of maintaining the mechanical strength of UAM metal structures, whilst also reducing the S_a , whilst ultrasonic deformed surfaces may degrade the mechanical performance under the same welding conditions.

According to previous work (Kong et al., 2005; Ram et al., 2006), a higher LWD typically results in a larger peeling resistance in UAM samples. However, this generalisation was not valid in this work. Although almost all the deformed samples exhibited higher LWD than undeformed ones, there was no evident increase in mechanical performance during the peel testing. For ultrasonic deformed samples, the peeling loads were even less than their undeformed counterparts when welded using the same UAM parameters. This suggested that although the deformation process could increase the LWD of the welding interface, there were still some areas where the metal foils were not metallurgically bonded and were only in intimate contact with one another. A potential cause for this lack of bonding could be due to surface modifying and work hardening of the substrate caused by the deformation process.

According to the bonding mechanisms of UAM described by Kong et al. [2] and Janaki Ram [14], the friction between mating surfaces and the plastic deformation of nascent metal beneath the oxide layer disrupts and displaces the hard oxide layer on the foil

surfaces and generates clean metal-metal contact points. Continuing plastic deformation drives metal flow to fill in the voids and achieve new contact points. Assisted by sonotrode pressure and ultrasonic oscillation, genuine metallurgical bonding can then be established at these metal-to-metal contact points. Successful welding is accomplished through the repeated and successive occurrence of these contact and potential bonding regions. Accordingly, besides UAM parameters two factors play an important role in the UAM process: surface roughness of the welding interfaces and surface hardness of the metal materials. A certain degree of surface roughness was desirable for enlarging the friction at the welding interface in order to disrupt the oxide layer. Moreover, heat generated in this period could result in small increases in ductility of aluminium alloy due to the thermal softening effect which could aid plastic deformation of the matrix material. Materials with lower hardness are preferable in UAM welding due to the ease of plastic deformation. Moreover, according to O'Brien's work (Jenney and O'Brien, 1991), the higher the ratio of oxide layer hardness to metal hardness, the easier it was to crack the oxide layer and thus the better the UAM welding. From the results shown in section 3.1, rolling deformation only acted to deform the peaks on the substrate surface and made limited modifications on the surface roughness and micro-hardness. This could explain its similar peel strength when compared to the undeformed samples. However, for ultrasonic deformed samples, the significantly smoothed surfaces and the increased micro-hardness led to decreased weldability and hence a lower peel strength.

3.3. Application in the direct embedding of electrical materials within solid metal parts

Based on results obtained in the previous sections, the rolling deformation process was adopted in the embedding of electronics within UAM metal matrices. Electrical circuitries comprising of base dielectric layers, silver conductor tracks, and encapsulating dielectric layers were deposited onto the undeformed and rolling deformed substrates using a bespoke screen using a DEK 265 Horizon screen printer (Fig. 15 (a)). The dielectric and conductive inks used in this work were 520 Series Soldermask made by Technic (Technic Company, 2008) and the C2131014D3 and C2050712P58 silver inks from Gwent Group (Gwent Group, 2011, 2013). All the inks were processed as recommended by the manufacturers. Following deposition, the printed circuitry was embedded via UAM encapsulation of an Al cover layer on the substrate (Fig. 15 (b)). The UAM parameter combinations used in this encapsulation were 800 N normal force, 15 μm sonotrode amplitude, and 10 mm/s welding speed.

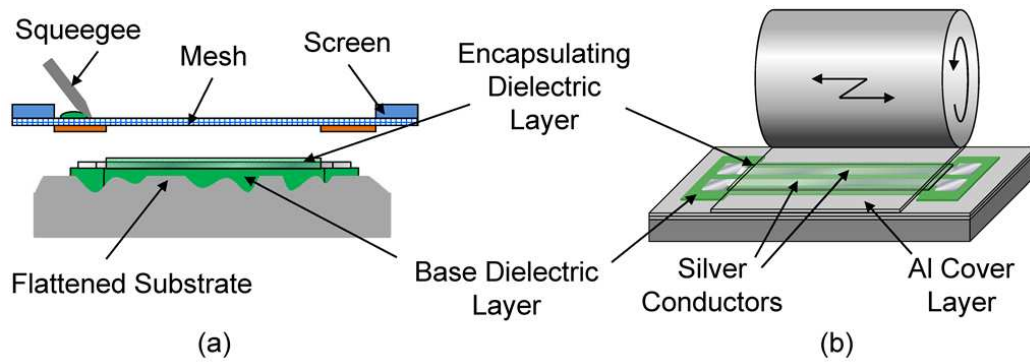


Fig. 15. Schematic diagram of UAM embedding of electronics within UAM metal matrices.

Finished samples were cross-sectioned and optical microscopy utilised for investigation in a similar method to that stated in Section 2.3.1 (Fig. 16). For undeformed and rolling deformed substrates, the electrical circuitries were successfully embedded within UAM metal matrices with no obvious deformation or fracture visible in the cross-sections of the printed circuitries. Fig. 16 (a) demonstrates the surface asperities which can arise on an undeformed substrate that could potentially penetrate the base dielectric layer and cause short connections between the silver conductor and the underlying bulk metal. In preliminary trials, these shortages were found in ~40% of these samples. In order to overcome these surface features, additional base dielectric layers must be deposited to achieve sufficient electrical insulation. This acts to increase the total thickness of printed circuitries and adversely affects the integrity of the UAM metal structures. These drawbacks could be overcome by the rolling deformation process. According to Fig. 16 (b), all the peaks were eliminated from the substrate surface and a single base layer was sufficiently thick enough to realise full insulation. This reduced the thickness of printed circuitries by ca. 25% and improved the integrity of the UAM metal matrix composite. The result of this is not only potential reductions in component mass (i.e. miniaturisation of embedded circuitries) but also reductions in processing times and material wastage.

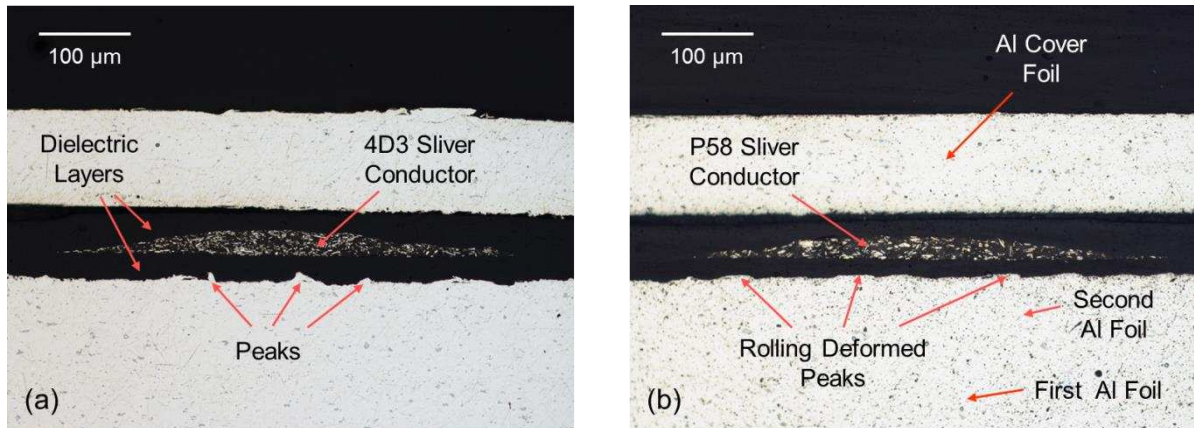


Fig. 16. (a) Cross-section of an embedded sample with undeformed substrate; (b) cross-section an embedded sample with rolling deformed substrate.

4. Conclusions

This work presents a combination of a surface deformation process and UAM that can be utilised in order to overcome the shorting problem which can arise during the embedding of printed electrical circuitry within UAM metal matrices.

Two types of surface deformation process were conducted in this work: Rolling Deformation (RD) and Ultrasonic Deformation (UD). Their modifications on surface topology and work hardening of UAM substrates were systematically investigated via non-contact focus variation microscopy and DB FIB-SEM respectively. By means of rolling the sonotrode over the substrate surface with an intermediary titanium layer, average surface roughness of UAM substrate could be decreased from 4.5 μm down to 4.1 μm. This could be further reduced to 0.8 μm by applying ultrasonic oscillation to this sonotrode in the ultrasonic deformation process. More significantly, the occurrence of large protruding peaks on the surface of the substrates could be removed via the application of the RD parameters. Through the grain refinement found in ion beam imaging, it was identified that UD samples displayed a high degree of work hardening as indicated by their substantial grain refinement in the upper regions of the foils surface. Their RD counterpart exhibited lesser degrees of refinement and it was concentrated in the regions local to the deformation of the surface peaks, leaving the bulk of the matrix unaffected.

The effect of deformed surfaces on mechanical strength of the resulting UAM structures was explored using optical microscopy and mechanical peel testing. Both deformation methods were able to improve the linear weld density of UAM structures (>10% increase). However, only substrates deformed via sonotrode rolling were able to maintain their peel strength of when compared to undeformed samples. Furthermore, substrates deformed using ultrasonic assistance acted to reduce the peel loads under same welding condition (>14% reduction in peeling load). This was attributed to both less degrees of work hardening of the matrix and a higher degree of

surface roughness; both of these factors are desirable for welding of successive foils via UAM. As a result, the rolling flattening process was considered to be a much more useful process and was applied in the construction of UAM MMC featuring embedded electronic structures.

As a result of this surface modification, the total thickness of the printed circuitry can be significantly reduced (reduction of ca. 25%) and thereby aids maintain the overall integrity of the UAM metal structures. This is important for realising novel multifunctional 3D metal matrix composites (MMC's) with embedded circuitries in application.

Acknowledgement

This work was supported by the Engineering and Physical Sciences Research Council, UK via the Centre for Innovative Manufacturing in Additive Manufacturing, grant number EP/I033335/2. We thank Mr. Jagpal Singh from the Loughborough University Metrology Laboratory and Mr. Scott Doak from Loughborough Materials Characterisation Centre (LMCC) for their support on topology measurement and FIB investigation, respectively.

Reference

- Friel, R.J. and Harris, R. a. (2010), "A nanometre-scale fibre-to-matrix interface characterization of an ultrasonically consolidated metal matrix composite", *Proceedings of the Institution of Mechanical Engineers, Part L: Journal of Materials: Design and Applications*, Vol. 224 No. 1, pp. 31–40.
- Gwent Group. (2011), "C2131014D3 Flexible Silver Ink", Technical Data Sheet.
- Gwent Group. (2013), "C2050712P58 Curable Silver Paste", Technical Data Sheet.
- Janaki Ram, G.D., Yang, Y. and Stucker, B.E. (2006), "Effect of process parameters on bond formation during ultrasonic consolidation of aluminum alloy 3003", *Journal of Manufacturing Systems*, Elsevier, Vol. 25 No. 3, pp. 221–238.
- Jenney, C.L. and O'Brien, A. (1991), *Welding Handbook*, American Welding Society, Vol. 1.
- Kong, C.Y. and Soar, R. (2005), "Method for embedding optical fibers in an aluminum matrix by ultrasonic consolidation.", *Applied Optics*, Vol. 44 No. 30, pp. 6325–6333.
- Kong, C.Y., Soar, R.C. and Dickens, P.M. (2004), "Optimum process parameters for ultrasonic consolidation of 3003 aluminium", *Journal of Materials Processing Technology*, Vol. 146 No. 2, pp. 181–187.
- Kong, C.Y., Soar, R.C. and Dickens, P.M. (2005), "A model for weld strength in ultrasonically consolidated components", *Proceedings of the Institution of Mechanical Engineers, Part C: Journal of Mechanical Engineering Science*, Vol. 219 No. 1, pp. 83–91.
- Kulakov, M. and Rack, H.J. (2009), "Control of 3003-H18 Aluminum Ultrasonic Consolidation", *Journal of Engineering Materials and Technology*, Vol. 131 No. 2, p. 021006.

- Li, D. and Soar, R.C. (2008), "Plastic flow and work hardening of Al alloy matrices during ultrasonic consolidation fibre embedding process", *Materials Science and Engineering: A*, Vol. 498 No. 1-2, pp. 421–429.
- Li, J., Monaghan, T., Bournias-Varotsis, A., Masurtschak, S., Friel, R.J. and Harris, R.A. (2014), "Exploring the Mechanical Performance and Material Structures of Integrated Electrical Circuits Within Solid State Metal Additive Manufacturing Matrices", *Proceedings of the 17th Annual Solid Freeform Fabrication Symposium, Texas*, pp. 857–864.
- Li, J., Monaghan, T., Masurtschak, S., Bournias-Varotsis, A., Friel, R.J. and Harris, R.A. (2015), "Exploring the mechanical strength of additively manufactured metal structures with embedded electrical materials", *Materials Science and Engineering: A*, Vol. 639, pp. 474–481.
- Monaghan, T., Capel, a. J., Christie, S.D., Harris, R. a. and Friel, R.J. (2015), "Solid-State Additive Manufacturing for Metallized Optical Fiber Integration", *Composites Part A: Applied Science and Manufacturing*, Vol. 76, pp. 181–193.
- Mou, C., Saffari, P., Li, D., Zhou, K., Zhang, L., Soar, R. and Bennion, I. (2009), "Smart structure sensors based on embedded fibre Bragg grating arrays in aluminium alloy matrix by ultrasonic consolidation", *Measurement Science and Technology*, Vol. 20 No. 3, p. 034013.
- Obielodan, J.O., Ceylan, a., Murr, L.E. and Stucker, B.E. (2010), "Multi-material bonding in ultrasonic consolidation", *Rapid Prototyping Journal*, Vol. 16 No. 3, pp. 180–188.
- Ram, G., Yang, Y., George, J., Robinson, C. and Stucker, B.E. (2006), "Improving Linear Weld Density in Ultrasonically Consolidated Parts", *Proceedings of the 17th Solid Freeform Fabrication Symposium*, pp. 692–708.
- Robinson, C.J., Stucker, B., Lopes, A.J., Wicker, R.B. and Palmer, J.A. (2006), "Integration of direct-write (DW) and ultrasonic consolidation (UC) technologies to create advanced structures with embedded electrical circuitry", *Proceedings of the 17th Annual Solid Freeform Fabrication Symposium, University of Texas at Austin, Austin, TX, Society of Manufacturing Engineers*, pp. 60–69.
- Siggard, E.J., Madhusoodanan, A.S., Stucker, B.E. and Eames, B. (2006), "Structurally Embedded Electrical Systems Using Ultrasonic Consolidation (UC)", *Proceedings of the 17th Solid Freeform Fabrication Symposium*, pp. 70–83.
- Smith, W. and Hashemi, J. (2006), *Foundations of Materials Science and Engineering*, McGraw-Hill, available at: <https://books.google.co.uk/books?id=1QUESgAACAAJ>.
- Technic Company. (2008), "520 SERIES Thermal 2 Pack Solder Resists", *Technical Data Sheet*.
- White, D.R. (2003), "Ultrasonic consolidation of aluminum tooling", *Advanced Materials & Processes*, ASM International, Vol. 161 No. 1, pp. 64–65.
- Yang, Y., Janaki Ram, G.D. and Stucker, B.E. (2010), "An analytical energy model for metal foil deposition in ultrasonic consolidation", *Rapid Prototyping Journal*, Vol. 16 No. 1, pp. 20–28.